

Multiscalar structural study of the ultramafic rocks of the Antrona Ophiolite (Pennine Alps)

Michele Zucali, Paola Tartarotti, Silvia Capelli, Bachir Ouladdiaf

Journal of the Virtual Explorer, Electronic Edition, ISSN 1441-8142, volume **41**, paper 4

In: (Eds.) Michele Zucali, Maria Iole Spalla, and Guido Gosso,
Multiscale structures and tectonic trajectories in active margins, 2012.

Download from: <http://virtualexplorer.com.au/article/2011/295/multiscalar-study-ultramafic-rocks-antrona-ophioli>

Click <http://virtualexplorer.com.au/subscribe/> to subscribe to the Journal of the Virtual Explorer.
Email team@virtualexplorer.com.au to contact a member of the Virtual Explorer team.

Copyright is shared by The Virtual Explorer Pty Ltd with authors of individual contributions. Individual authors may use a single figure and/or a table and/or a brief paragraph or two of text in a subsequent work, provided this work is of a scientific nature, and intended for use in a learned journal, book or other peer reviewed publication. Copies of this article may be made in unlimited numbers for use in a classroom, to further education and science. The Virtual Explorer Pty Ltd is a scientific publisher and intends that appropriate professional standards be met in any of its publications.

Multiscalar structural study of the ultramafic rocks of the Antrona Ophiolite (Pennine Alps)

Michele Zucali

1. Università degli Studi di Milano, Dipartimento di Scienze della Terra, via Mangiagalli, 34-20133 Milano (Italy).
Email: michele.zucali@unimi.it
2. CNR-IDPA - Sezione di Milano, Via Mangiagalli 34 - 20133 – Milano, Italy.

Paola Tartarotti

1. Università degli Studi di Milano, Dipartimento di Scienze della Terra, via Mangiagalli, 34-20133 Milano (Italy).
2. CNR-IDPA - Sezione di Milano, Via Mangiagalli 34 - 20133 – Milano, Italy.

Silvia Capelli

Institut Laue-Langevin, rue J. Horowitz 38042 Grenoble Cedex 9, France.

Bachir Ouladdiaf

Institut Laue-Langevin, rue J. Horowitz 38042 Grenoble Cedex 9, France.

Abstract: In the Alpine nappe stack, the Antrona Ophiolite (Italian side of the Western Central Alps) is sandwiched between the overlying continental Monte Rosa Nappe (upper Penninic domain) and the underlying Camughera-Moncucco continental Unit (middle Penninic). The ophiolite sequence includes ultramafic rocks, metagabbros and mafic rocks covered by calcschists. Ultramafites constitute a huge body of serpentised peridotites including interbedded layers of gabbros, clinopyroxene-rich and amphibole-rich rocks, and chloriteschist. In spite of the Alpine tectonic and metamorphic reworking, the ultramafic portion of the Antrona Ophiolite still preserves relict textures and minerals that can be referred to the pre-Alpine or early Alpine evolution. A detailed microstructural analysis performed at polarised microscope and SEM on less serpentised, olivine-rich samples is here presented. It is integrated with a quantitative textural analysis of Lattice Preferred Orientation (LPO) by neutron diffraction acquired on selected samples of olivine-rich samples. The results allow to infer a mantle origin for the ultramafic rocks, suggesting T conditions > 800°C for the activation of slip systems in olivine.

Introduction

The Antrona ophiolite consists of serpentized ultramafites, metagabbros and mafic rocks (metavolcanics) covered by calcschists (Colombi and Pfeifer, 1986; Pfeifer *et al.*, 1989; Carrupt and Schulp, 1998; Turco and Tartarotti, 2006). The internal setting and stratigraphy of the Antrona ophiolite are still not well constrained, probably due to the small extent and pervasive metamorphic retrogression. Consequently, these ophiolites have been often neglected and poorly considered for the paleogeographic reconstruction of the Western Tethys. The ultramafites of the Antrona ophiolite have recently been investigated (Tartarotti *et al.*, 2011). The microstructural and microchemical features of these rocks have led these Authors to interpret this ophiolite portion as deriving from original mantle harzburgites and/or lherzolites associated with dunite pods and (possibly) pyroxenite layers. These rocks partly retain either the original chemistry or the effect of oceanic hydrothermal alteration (Tartarotti *et al.*, 2011). The Antrona ophiolite thus represents remnants of the oceanic lithosphere of the Mesozoic western Tethys, now inserted as tectonic slices in the Penninic nappe pile of the western Central Alps. The Alpine tectono-metamorphic evolution of the ophiolite is characterized by a subduction-related blueschist prograde path, followed by high-pressure (eclogitic) metamorphic peak, and subsequent retrograde exhumation dominated by epidote-amphibolite to amphibolite facies conditions (Colombi and Pfeifer, 1986; Pfeifer *et al.*, 1989; Carrupt and Schulp, 1998; Turco and Tartarotti, 2006). In this paper, we have addressed our investigations to the microstructural features of mantle olivine and spinel still preserved in less serpentized peridotite samples. The microstructural study is complemented by a quantitative texture analysis by neutron diffraction on selected olivine-rich samples, to investigate the lattice preferred orientations (LPO) of relict fresh olivine. Quantitative study of LPO in natural rocks is of great interest if one wants to infer the conditions of deformation of crystalline aggregates or unravel multiple stages of recrystallization producing distorted lattices (Gatta *et al.* 2009). The resulting olivine LPO will be compared with experimental and natural observations on lattice orientations of olivine (Karato, 2008 and reference therein). We use the quantitative LPO study of relict olivine to constraint the deformation mechanisms active during the development of fabrics

predating the S_2 foliation and relate them to the pre-Alpine evolution, from the mantle to oceanic stages.

Geological setting

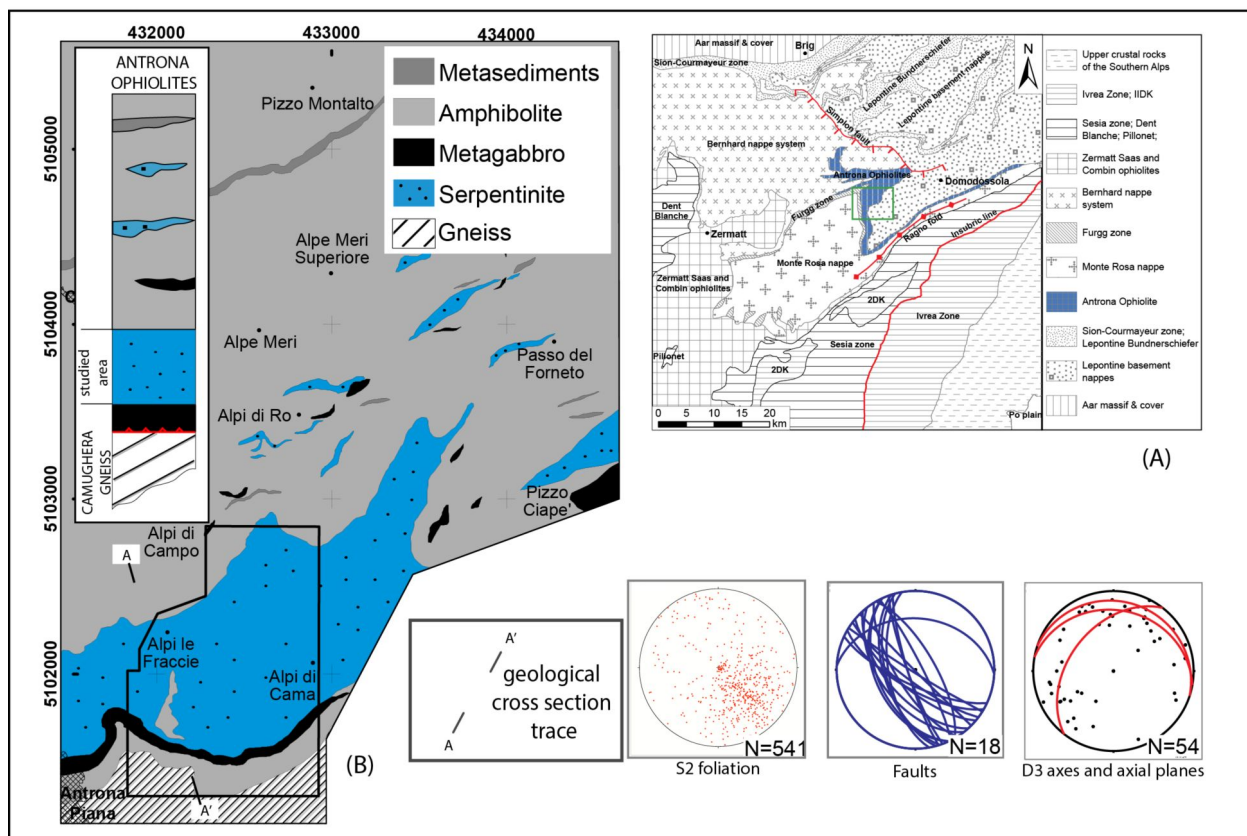
The Antrona Ophiolite is located in the Pennine Alps (western part of the Central Alps; Fig. 1). On the Italian side, the Antrona ophiolite crops out in the Antrona, Loranco, Bognanco, Anzasca, and Vigizzo valleys, near Domodossola; on the Swiss side, it is exposed in the Lagginatal-Simplon area, to the south of the Simplon Line. In the internal Pennine domain, the Antrona ophiolite lies on the footwall of the huge Monte Rosa recumbent anticline (upper Penninic) where it forms two large-scale structures, i.e., the Antrona synform (or Gabbio synform) and the Vanzone antiform (Laduron and Merlin, 1974; Milnes *et al.*, 1981). The tectonic contact between the Antrona ophiolite and the Monte Rosa unit is underlined by the Furgg Zone (Argand, 1911; Bearth, 1954; Jaboyedoff *et al.*, 1996; Escher *et al.*, 1997; Froitzheim, 1997, 2001; Keller and Schmid, 2001; Steck *et al.*, 2001; Kramer, 2002) consisting of micaschists, albitic schists, and leucocratic gneisses (Permian-Carboniferous) with eclogitic to greenschist-facies mafic boudins, thin micaceous quartzites and dolomitic marbles of probable pre-Mesozoic age (Bearth, 1954). The Monte Rosa anticline is wrapped at its top by the Zermatt-Saas ophiolite nappe (e.g., Ernst and Dal Piaz, 1978; Oberhansli, 1980; Barnicoat and Fry, 1986; Reinecke, 1991, 1998; Bucher *et al.*, 2005; Angiboust *et al.*, 2009) which disappears at depth below the middle Penninic Mischabel backfold (Milnes *et al.*, 1981). The Antrona Ophiolite overlays the middle Penninic Camughera-Moncucco Nappe (included in the "Leptontine basement nappes" of Fig. 1; Bearth, 1956; Laduron, 1976; Bigioggero *et al.*, 1981; Milnes *et al.*, 1981; Escher *et al.*, 1997; Steck *et al.*, 1997; Keller *et al.*, 2005a). The Antrona ophiolite consists of N-MORB to T-MORB-type metabasalts retaining relict pillow structures, minor serpentinite, and gabbro (Laduron, 1976; Laduron and Merlin, 1974; Colombi and Pfeifer, 1986; Colombi, 1989; Pfeifer *et al.*, 1989; Martin *et al.*, 1994; Carrupt and Schulp, 1998; Turco and Tartarotti, 2006). These rocks are covered by garnet-micaschists, metaradiolarite, calcschists, sedimentary breccia, marbles, and graphitic marbles. These ophiolitic rocks have experienced regional subduction-related high-pressure metamorphism during the Alpine orogeny (Colombi and Pfeifer, 1986; Keller *et al.*, 2005a; Keller *et al.*, 2005b; Turco and

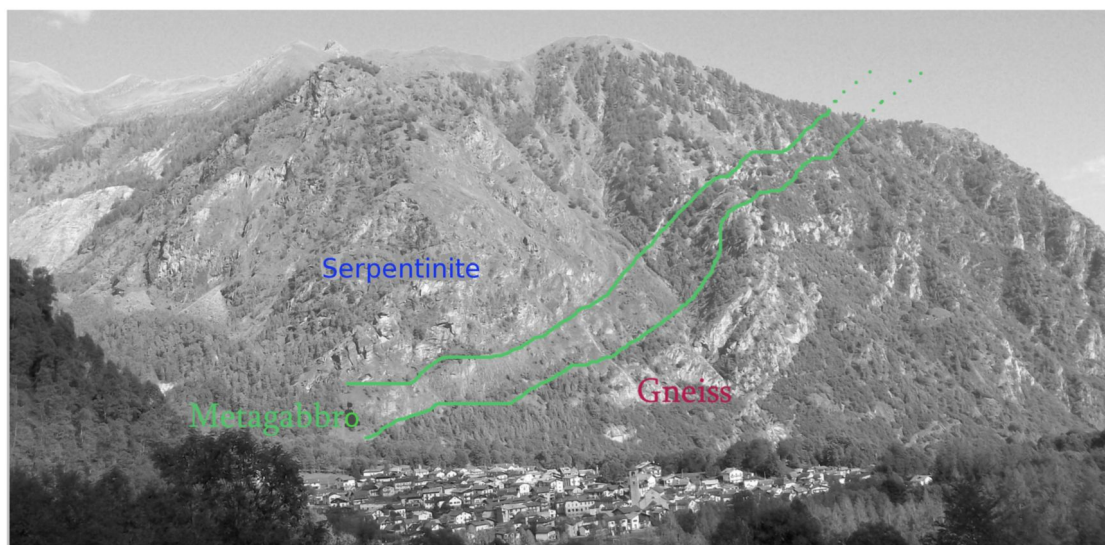
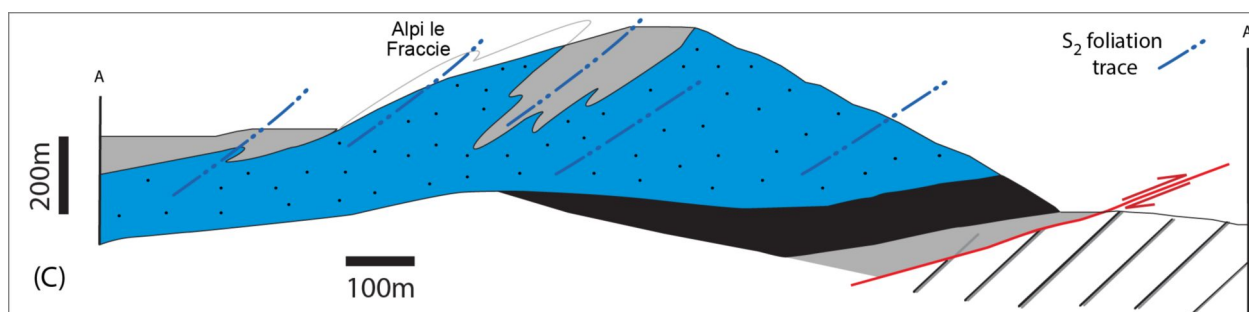
Tartarotti, 2006). Eclogite rocks in the Antrona ophiolite have been documented by Colombi and Pfeifer (1986) and Turco and Tartarotti (2006). The occurrence of lawsonite pseudomorphs within amphibolites have led Turco and Tartarotti (2006) to suggest a qualitative P-T evolution characterized by early Alpine prograde blueschist path followed by a high pressure (eclogitic) metamorphic peak. P-T estimates for the metamorphic peak give $T = 372^{\circ} \text{C}$ for $P = 1 \text{ GPa}$ and $T = 386^{\circ} \text{C}$ for $P = 1.5 \text{ GPa}$ (Turco and Tartarotti, 2006). During the decompression accompanying the exhumation history in the Tertiary, the Antrona ophiolite was re-equilibrated under epidote-amphibolite to amphibolite facies conditions (Pfeifer *et al.* 1989; Turco and Tartarotti, 2006).

Mesostructure of the Antrona ultramafic rocks

The ultramafic portion of the Antrona ophiolite is exposed near the village of Antronapiana where it forms a ca. 35 km² wide massif (Fig. 1). The ultramafic rocks underlie amphibolites and metasediments, thus constituting a sole for the volcanic and cover portion of the ophiolite sequence. In their marginal parts, the ultramafic rocks are in contact with flaser metagabbro grading to mylonitic amphibolite near the main tectonic contact with the Middle Penninic Camughera-Moncucco unit, here consisting of orthogneiss (Fig. 1).

Figure 1. Mesostructure of the Antrona ultramafic rocks





A) Tectonic map of the North-eastern Pennine Alps with location of the Antrona ophiolite; B) Simplified geologic map of the Antrona ophiolite with location of the geological cross section; C) Geological cross section through the Antrona ophiolite and the underlying Camughera gneiss; D) Panoramic view of the Antrona ophiolite – Camughera gneiss contact. Stereographic plots of S_2 foliation, faults, and D_3 fold axes are reported (see text). (Modified after Tartarotti et al., 2011).

The ultramafic rocks are represented by serpentinite, dunite, amphibole-rich rocks, and chloriteschist. Dunite occurs as dm-thick layers or pods parallel to the serpentinite foliation. The amphibole-rich rocks form dm-thick and few meters-long layers concordant with the serpentinite foliation (see Fig. 2). The contact between these layers and serpentinite is marked by chloriteschist. Chloriteschists also occur as isolated layers within the serpentinite or they are associated to amphibole+chlorite-rich layers. The main ultramafic rock is indeed represented by serpentinite, commonly characterized by a weak foliation and fine grainsize. Mylonitic serpentinites occur near the border of the ultramafic massif. Serpentinites include mm- to cm-sized layers of mafic/ultramafic rock. The following types of rocks interbedded within serpentinites were distinguished in the field: a) millimetric brownish ol

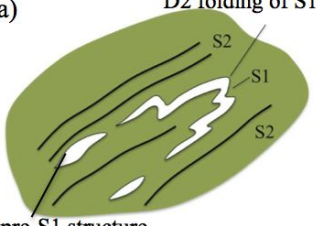
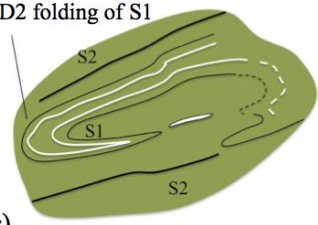
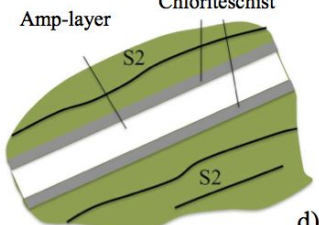
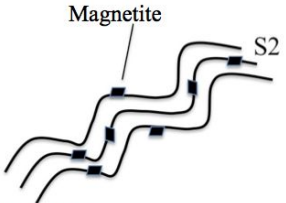
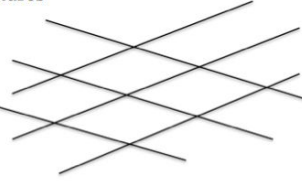
+cpx-layers (Fig. 2a); b) millimetric boudins or lozenge-shaped cpx+amp±chl±mag-aggregate (Fig. 2b); c) centimetric white-to-greenish cpx-rich layers transposed within the serpentinite foliation (Fig. 2c).

The most pervasive foliations recognizable at the scale of the outcrops (S_1 and S_2) are developed in the entire ophiolitic section and are related to different stages of the Alpine evolution. In the ultramafic rocks, S_2 is mainly defined by antigorite and magnetite; S_1 is recorded by the ol+cpx-layers and cpx-rich layers infolded in the serpentinite and forming tight or isoclinal folds (mostly detectable under the microscope) within the S_2 foliation (Figs. 2a and 2c). S_1 foliation is attributed to D_1 deformation. Isoclinal folding of S_1 and development of the S_2 foliation are ascribed to D_2 deformation (Figs. 2a and 2c), which is also responsible for mylonitization of serpentinite near the border of the massif. S_1 and S_2 foliations are then overprinted by D_3 deformation generating

crenulation or chevron folds (Fig. 2e), commonly concentrated near the contact between serpentinites and harder mafic rocks. D3 folds do not develop axial plane foliation visible at the outcrop scale but concur to the high dispersion of S_2 data (see Fig. 1). Late, brittle D4

deformation is characterized by diffuse S-C type structures and fractures overprinting all previous structures, commonly generating lozenge-shaped rock volumes at all scales especially in serpentinites and in calc-schists (Fig. 2f).

Figure 2. Main mesostructural features of the Antrona ophiolite.

PHASE	SERPENTINITE	PICTURES
D1+D2	a) D2 folding of S1 pre-S1 structure 	
	b) lozenge-shaped mineral aggregate 	
	c) D2 folding of S1 	
	d) Amp-layer Chloriteschist 	
D3	e) Magnetite D3 crenulation of S2 foliation 	
D4	f) D4 fractures 	

A) to C): Main structures related to the D_1 and D_2 deformation phases. D) Amphibole-rich layer concordant with the serpentinite (S_2) foliation). E) and F) refers to structures related to late D_3 and D_4 phases. Pictures on the right side show representative outcrops of structures described on the left. D = deformation; S = foliation.

Microstructure and mineral chemistry

Thin-section investigations were addressed to characterizing the petrography and microstructure of the Antrona ultramafic rocks. The main rock types are:

serpentinized peridotite (both foliated and mylonitic serpentinites), clinopyroxene-rich layers (infolded within serpentinite), chloriteschists, coarse-grained peridotite,

dunite, and amphibole-rich layer. In all rocks we observed a main penetrative foliation that we called S_2 on the basis of the proposed microstructural evolution. S_2 foliation thus constitutes a fundamental reference point in the structural reconstruction.

In serpentinites, S_2 foliation is mainly defined by serpentine. In some foliated serpentinites, S_2 is marked by millimetric boudins or lozenge-shaped aggregates of fine-grained cpx+amp±chl+mag interpreted as deriving by replacement of earlier clinopyroxene, since relict clinopyroxene porphyroclasts are still locally recognizable inside the mineral aggregate. Consequently, the lozenge-shaped aggregates (see Fig. 2b), although now oriented parallel to S_2 structures, may represent relict pre- S_2 structures. Mylonitic serpentinites are made of serpentine, magnetite, and carbonate. Serpentine crystals with SPO mark the mylonitic S_2 foliation often deformed by small-scale D3 crenulation (see also Fig. 2e). Ca-carbonate occurs as millimetric porphyroblasts showing intracrystalline deformation as well as smaller grains distributed in the serpentine groundmass.

In the cpx-rich layers transposed within the serpentinite (see Fig. 2c), the S_2 is marked by fine-grained neoblastic clinopyroxene, sometimes with polygonal or mosaic-texture.

In chloriteschists, S_2 foliation is defined by chlorite and amphibole crystals and is superimposed by incipient S_3 foliation.

In coarse-grained peridotite and in dunites, S_2 foliation is not visible and the static growth of chl±amp±srp is the only microstructure likely related to D_2 stage.

The amphibole-rich layers consist of fine-grained aggregates of amphibole (~80%) and minor plagioclase and sphene oriented parallel to the S_2 foliation. Few sub-millimetric anhedral crystals of amphibole or chlorite (pseudomorphs?) were observed in the fine-grained groundmass.

Post- S_2 structures are represented by coarse-grained acicular crystals of serpentine or amphibole, which define an incipient and discontinuous S_3 foliation, superimposed to the main foliation S_2 , and by veins. Veins are widespread in serpentinite and chloriteschists and are commonly filled with serpentine or chlorite fibres. All vein types crosscut all other structures, and are then later than pervasive S_2 and incipient S_3 foliations.

Microstructures older than S_2 were observed in most fresh rocks and were used to unravel the oldest

metamorphic evolution. These structures include S_1 and pre- S_1 structures.

S_1 structures are mainly represented by relict foliations infolded within the S_2 foliation. In serpentinized peridotites, S_1 foliation is marked by sub-millimetric layers of neoblastic olivine and clinopyroxene replacing former olivine (Fo₈₇₋₈₈) and clinopyroxene porphyroblasts (Wo₅₀-En₄₇-Fs₃), respectively, still occurring in less recrystallized samples. These layers correspond to the brownish ol+cpx-layers recognized in the field and infolded within the serpentine S_2 foliation (see Fig. 2a). In clinopyroxene-rich layers (see Fig. 2c), clinopyroxene shows three different textures: relict porphyroclast containing exsolution lamellae often filled with opaque minerals, mm-sized diopside porphyroblasts, often arranged in fan-shaped aggregates showing wavy extinction, and fine-grained granoblastic-neoblastic diopside, showing polygonal or mosaic-texture. Porphyroblastic diopside is here interpreted as relict S_1 whilst porphyroclastic exolved clinopyroxene could be a pre- S_1 structure.

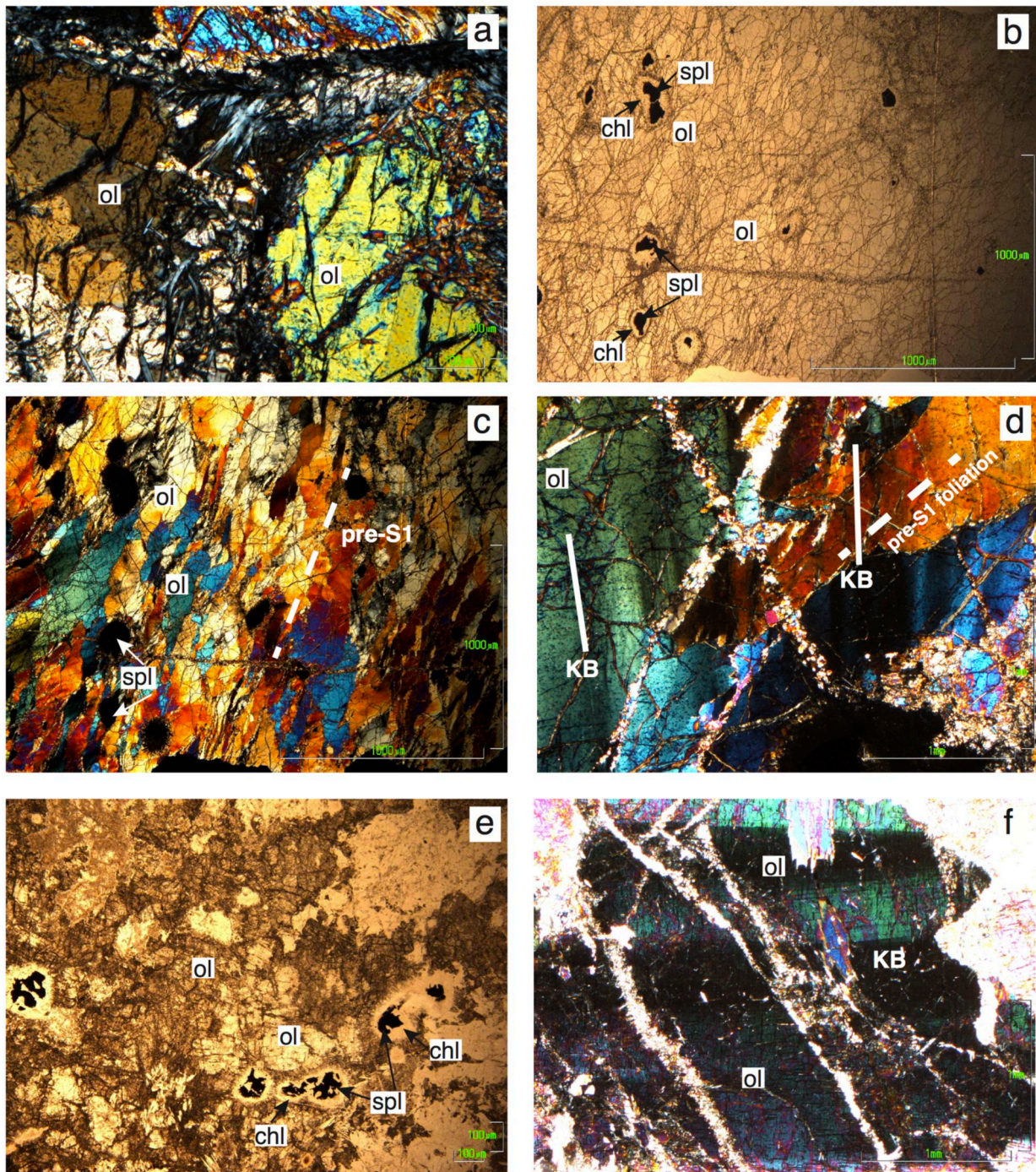
Pre- S_1 structures are the oldest evidence of the tectono-metamorphic evolution recorded by the studied rocks and thus represent a key for unravelling the nature of their protolith (Fig. 3b and c). In serpentinites, pre- S_1 structures are represented by: relict exolved clinopyroxene porphyroclasts (see above), olivine porphyroblasts, spinel porphyroclasts, and by lens-shaped or rectangular pseudomorph sites of serpentine, probably replacing an earlier igneous mineral (pyroxene). In the least serpentinized samples, pre- S_1 structure is attested by olivine occurring as round-shaped millimetric porphyroblasts (Fig. 3a). Olivine porphyroblasts commonly show intracrystalline deformation attested by the presence of wavy extinction and subgrain boundaries (or “kink-bands” = KB; Mercier and Nicolas 1975; Fig. 3a). Dunite layers and pods consist of olivine, spinel, opaque minerals, chlorite, ± serpentine (Fig. 3b, 3c). This rock is fine-grained, so no clear foliation is visible in the field. Under the microscope, dunite reveals the occurrence of a foliation marked by the shape-preferred orientation (SPO) of olivine porphyroblasts, commonly elongated and strained (Fig. 3c). Intracrystalline deformation is attested by the presence of kink-bands (“KB” in Fig. 3d). The angle between foliation and kink-bands boundaries (KBB) is about 45°. We interpret this foliation as a “pre- S_1 ” structure. Olivine neoblasts in dunite grow at the rim of olivine porphyroblasts (both are Fo90), but more often they fill

intercrystalline fractures in association with serpentine crystals (Fig. 3d). Spinel occurs as mm-sized holly-leaf shaped crystals or ovoidal porphyroclasts mantled by a chlorite rim (see Fig. 3b). BSE images of spinel (Fig. 4) show that in dunite spinel is characterized by a “porous” texture, as defined by Merlini *et al.* (2009). Spinel has a ferritchromite composition (Cr_2O_3 wt% ~ 55 ; FeO_{tot} wt% ranging from ca. 35 to 37; see also Tartarotti *et al.*, 2011). Element maps show the compositional variations of porous ferritchromite. The presence of Si, Mg, and scarce Al in the interstitial space visible in the maps suggest the occurrence of a silicate (serpentine? chlorite? undetectable due to its fine grain-size) forming intergrowths with spinel. Chlorite rimming the spinel crystals has Cr_2O_3 wt% content of up to 0.4; see also Tartarotti *et al.*, 2011).

Coarse-grained ol+cpx+spl (\pm amp, \pm chl)-rich rocks are characterized by olivine, clinopyroxene, pseudomorphic aggregates after probable orthopyroxene, and spinel (Fig. 3e). Olivine occurs as mm-sized olivine porphyroblasts (Fo_{87-88}) showing intracrystalline deformation and

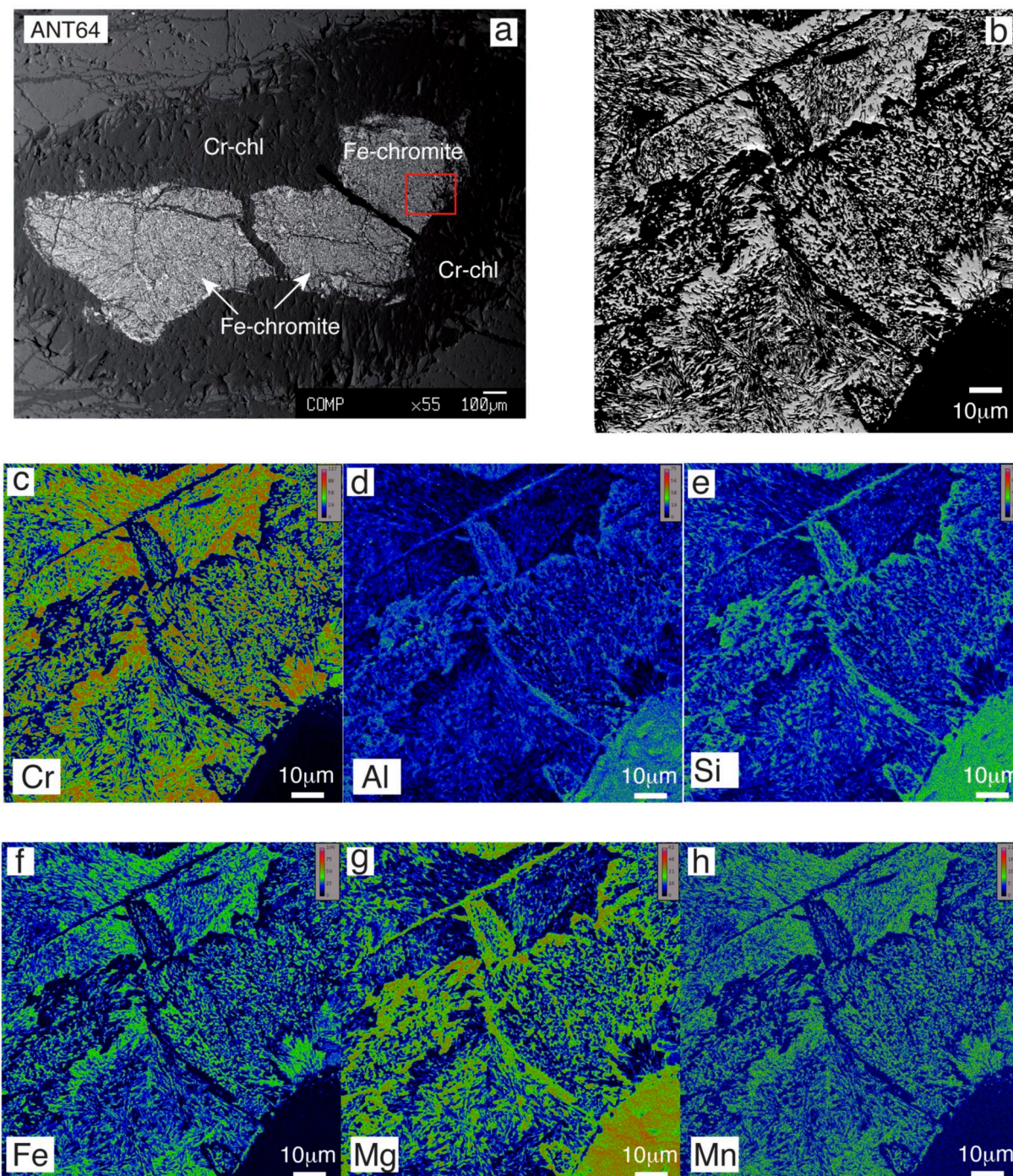
olivine neoblasts (Fig. 3f), relict clinopyroxene porphyroclasts, and mm-scale chl+amp pseudomorphs (replacing orthopyroxene?). Spinel crystals are sub-millimetric and their shape recalls the holly-leaf habit described in mantle-derived peridotites (e.g., Mercier and Nicolas, 1975; Nicolas and Poirier, 1976). Spinel is always rimmed by a thick corona of chlorite. BSE images of spinel in these coarse-grained ol+cpx+spl-rich rocks (Fig. 5) show that spinel is characterized by a “porous” texture, similarly to the dunite spinel. Spinel has a ferritchromite composition (Cr_2O_3 wt% ranging from ca. 53 to 57; FeO_{tot} wt% ranging from 35 to 39; see also Tartarotti *et al.*, 2011). Element maps show the compositional variations of porous ferritchromite. The presence of Si, Al, Mg, Fe, and Mn in the interstitial space visible in the maps suggest the occurrence of chlorite, forming fine-grained intergrowths with spinel. Chlorite at the spinel rim has a Cr-chlorite composition (Cr_2O_3 wt% up to 1; see Tartarotti *et al.*, 2011).

Figure 3. Photomicrographs of representative samples of the Antrona ultramafic rocks.



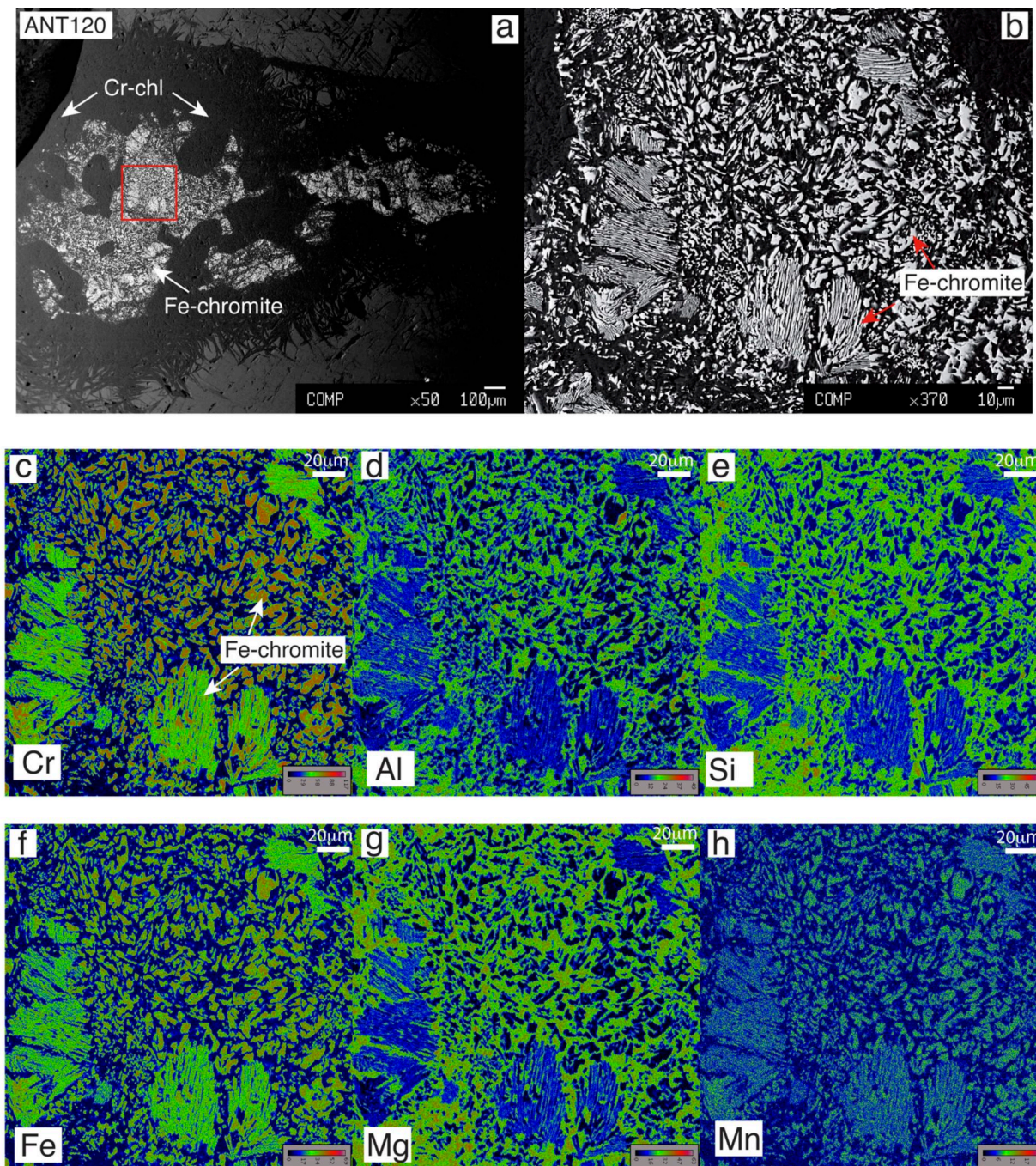
a) Olivine porphyroblasts (ol) with intracrystalline deformation; crossed nicols. b) General view of dunite (sample ATN64) with olivine and spinel porphyroblasts rimmed by chlorite; plane-polarised light. d) Elongate, coarse-grained olivine porphyroblasts (ol) showing intracrystalline deformation, and spinel in fresh dunite (sample ANT64). Olivine shape preferred orientation almost coincides with rock foliation pre-S₁ (see text); crossed nicols. d) Detail of dunite ANT64: coarse-grained elongated olivine porphyroblasts (ol) cut by veins filled with fine-grained olivine neoblasts. Orientation of internal kink-bands in olivine porphyroblasts (KB) describes an angle of about 45° with the rock foliation (pre-S₁ foliation); crossed nicols. e) General view of olivine and spinel in coarse-grained ol+cpx+spl (±amp, ±chl)-rich rock (sample ANT120). Spinel is rimmed by chlorite corona; plane-polarised light. f) Detail of sample ANT120 showing kink-bands (KB) due to intracrystalline deformation of olivine porphyroblasts; crossed nicols.

Figure 4. BSE images and X-ray element maps of spinel porphyroclast in dunite (sample ANT64).



Microchemical analyses of spinel are reported in Tartarotti et al. (2011). a) SEM image showing a general view of spinel (ferritchromite) porphyroclast rimmed by Cr-chlorite. b) Detail of picture (a) illustrating the "porous" texture of ferritchromite consisting of fine-grained intergrowths of spinel and an unknown mineral. c-h) X-ray element maps showing the distribution of Cr, Al, Si, Fe, Mg, and Mn in the same crystal portion as illustrated in (b). Bright warm colors correspond to high concentrations; dark blue colors correspond to low concentrations. Ferritchromite is made of fine-grained intergrowths of spinel and an unknown mineral. The presence of Si, Mg, and scarce Al suggest that this mineral could be serpentine or chlorite; however it is not detectable due to its fine grain-size. Element maps performed at the by using a JEOL JXA-8200 probe, equipped with five WDS spectrometers and an EDS spectrometer, at the Dipartimento di Scienze della Terra "Ardito Desio" of the University of Milan.

Figure 5. BSE images and X-ray element maps of spinel porphyroclast in coarse-grained ol+cpx+spl-rich rock (sample ANT120).



Microchemical analyses of spinel are reported in Tartarotti et al. (2011). a) SEM image showing a general view of spinel (ferritchromite) porphyroclast rimmed by Cr-chlorite. b) Detail of picture (a) illustrating the “porous” texture of ferritchromite consisting of fine-grained intergrowths of spinel and an unknown mineral. c-h) X-ray element maps show the distribution of Cr, Al, Si, Fe, Mg, and Mn in the same crystal portion as illustrated in (b). Bright warm colors correspond to high concentrations; dark blue colors correspond to low concentrations. Ferritchromite is made of fine-grained intergrowths of spinel and an unknown mineral. The presence of Si, Mg, and scarce Al suggest that this mineral could be serpentine or chlorite; however, it is not detectable due to its fine grain-size. Element maps performed at the by using a JEOL JXA-8200 probe, equipped with five WDS spectrometers and an EDS spectrometer, at the Dipartimento di Scienze della Terra “Ardito Desio” of the University of Milan.

The coarse-grained ol+cpx+spl-rich rocks are recrystallized at various extents into amp (tremolite)+chl-rich rocks, the resulting mineral assemblage and foliation thus depending on the extent of rock recrystallization.

Summing up, the porphyroblastic olivine, clinopyroxene, and spinel in less serpentinized peridotite, in dunite, and in coarse-grained ol+cpx+spl-rich rocks can be attributed to a pre-S₁ structure representing the remnant of early, porphyroclastic mantle-derived texture (sensu Mercier and Nicolas, 1975). This pre-S₁ structure has been overprinted by S₁ structures as described above.

Lattice Preferred Orientation (texture) quantitative analysis by neutron diffraction

Quantitative texture analysis is used to determine the statistical distribution of crystal lattice planes orientations within a rock, separating the components related to each mineral family contribution. The crystallographic (lattice) preferred orientation (LPO) of rock-forming minerals is then used as indicator not only of the strain state during the LPO development but also of the pressure and temperature conditions, relating the observed LPO patterns to those reported in literature from experimental, natural observations or numerical simulations (Karato, 2008; Tommasi *et al.* 2000; Warren *et al.*, 2008). In the following paragraphs, the results from a LPO study of three samples will be shown; the samples have been selected among those preserving the best relics of olivine crystals, providing a good material to relate LPO with the physical conditions under which olivine aggregates have grown or were deformed.

Description of studied samples

ANT64 – Foliated olivine (90%) + spinel (5%) + chlorite (5%) peridotite

ANT64 is a dunite mainly consisting of olivine (Ol 90%), while opaque minerals, chlorite, ± serpentine constitute less than 10% of the rock. The pre-S₁ foliation is defined by the shape-preferred orientation of olivine. Olivine occurs as elongated porphyroblasts, locally strongly strained (Ol_p) and rimmed by fine aggregates of newly-formed olivine neoblasts (Ol_n) (see Fig. 3).

ANT138 – Massive olivine (60%) + orthopyroxene/clinopyroxene (30%) + spinel (10%)

ANT138 is a massive peridotite partly replaced by chlorite and amphibole. The original porphyroclastic texture is still shown by olivine large grains (1-2mm) and pyroxene domains. Spinel grains occur as partly replaced

domains where the original spinel grains are rimmed by aggregates of chlorite. A gentle SPO of olivine grains occurs also associated with undulose extinction and lamellae.

ANT120 – Massive olivine (40%) + amphibole (30-35%) + chlorite (20%) peridotite

ANT120 is a massive, coarse-grained peridotite partly replaced by aggregates of amphibole and chlorite. Relics of olivine occur as large (1-2mm) porphyroclasts rimmed by thin aggregates of chlorite and amphibole. Amphibole also occurs as large grains not showing preferred orientation. Relicts of original olivine peridotite are wrapped by layers of fine grained amphibole + chlorite. Olivine commonly shows undulose extinction and sub-grains (<1mm).

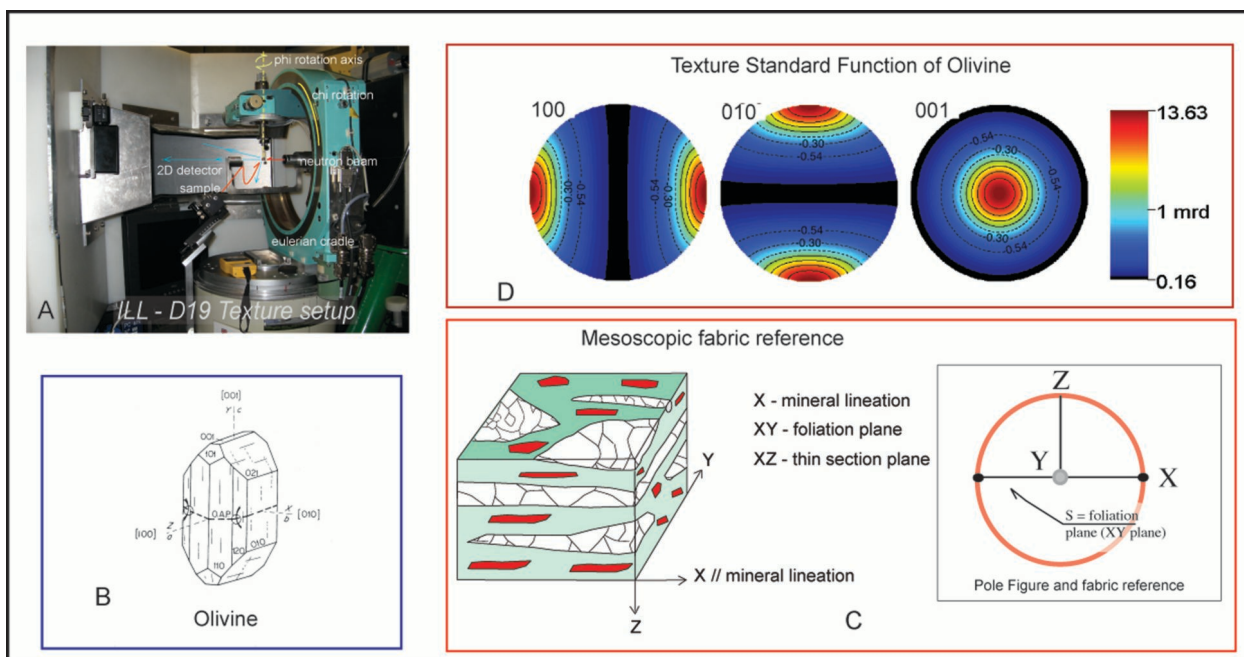
Method

In order to quantify the LPO of minerals, a neutron diffraction technique was used. This technique allows us to investigate volumes of rock of $\approx 1 \text{ cm}^3$ -volume in a short time (about 1-2 hours), thanks to the penetration of neutron in matter and to the high flux, available at the nuclear reactor at the Institute Laue-Langevin (Grenoble, France). The samples were measured at D19 diffractometer (www.ill.eu/instruments-support/instruments-groups/instruments/d19/), which covers an angular range of 120°x30° with spatial resolution of 0.19° horizontally and 0.12° vertically. The detecting columns cover an equivalent χ -range of 30° to 60°, for a total detecting solid angle of roughly 1.1 sr. A wavelength of 1.46 Å was used; the data reduction strategy consisted of intensity corrections, localisation corrections and combined analysis. This instrument is located as close to the neutron source, and the flux at the sample position is between 10⁷ to 10⁸ ncm⁻²s⁻¹. More details about the experimental and beamline setup have been already described elsewhere (D1B beamline: Camana *et al.*, 2002; Zucali *et al.*, 2002; D19 beamline: Zucali *et al.*, 2010; Tartarotti *et al.*, 2011). More details about LPO analysis using neutron or X-ray diffraction may be found in the following literature (Bunge *et al.*, 1982; Wenk, 1985; Heizmann and Laruelle, 1986; Ullemeyer *et al.*, 1998; Wenk *et al.* 1994; Matthies *et al.*, 1997; Morawiec, 2004; Chateigner, 2010). Figure 6 reports the main setup of D19 beamline as well sample references used for texture analysis as mesoscopic fabric axes, crystallographic axes of olivine and Texture Standard Functions of Olivine produced

using lattice parameters and a triclinic symmetry of the sample. Texture Standard Functions correspond to the PFs of the distribution of the main crystallographic axes of olivine, with respect to mesoscopic fabric axes, as produced by a single crystal. In Figure 6 are also reported the orientation of mesoscopic fabric axes with respect to

PFs; in particular, all PFs for samples ANT64, ANT138 and ANT120 are referenced to the mesoscopic foliation plane (XY plane), where X direction is the mineral lineation, represented by the horizontal line in the PFs. The normal to the foliation plane plots at the north pole of the PF.

Figure 6. ILL -D19 diffractometer setup and sample mesoscopic and pole figure references.



A) D19 setup showing the incident and diffracted beam directions with respect to the eulerian cradle and position sensitive detector; B) Olivine crystal structure; C) Mesoscopic fabric references: X, Y and Z axes are shown in rock sample and pole figure representation. D) Texture Standard Function pole figure of olivine single crystal as represented by Maud. Triclinic sample symmetry is used.

Results

Olivine LPO was investigated and results are shown in figures 7 and 8 and table 1. Table 1, in particular, reports main parameters resulting from each sample refinement, including estimates of the texture refinement qualities, where RW and RB correspond to weighted and Bragg factors for ODF analysis (Chateigner, 2010); the F2 factor (i.e. the texture factor) is an estimate of the overall LPO strength (Bunge and Esling, 1982); this latter decreases from ANT64 to ANT138. One should, however, bear in mind that F2 is largely influenced by the texture kind and crystal phase. GoF (Goodness of Fit) also describes the quality of the refinement (Toby, 2006) and its values are reported in Table 1. The Quantitative

Texture Analysis was performed on two samples of massive peridotite and one sample of foliated dunite. In the three samples LPO analysis was performed on olivine since it is the only preserved mineral constituting the pre-S₁ fabrics. Figure 7 reports the comparison of experimental and recalculated PFs of selected crystallographic planes. Where samples are characterized by a planar fabric, the macroscopic foliation (XY plane), is taken as the main reference to the pole figures geometry, as shown in figure 8. Olivine has an orthorhombic structure, space group Pbnm (N. 62) and the cell parameters, used for the profile fitting and E-WIMV (Matthies and Vinel, 1982; Liu *et al.* 1993), are a=4.77 Å, b=10.20 Å, c=6.00 Å.

Table 1. D19@ILL Years 2009-2010

Sample	Rock Type	Minerals	Rw	Rb	GoF(sigma)	F2 (olive)	LPO type	Grain-size (µm)
ANT64	foliated dunite	ol+sp	25.59	18.79	1.37	3.43	E-D	50-300
ANT120	massive dunite	ol+cpx/opx +sp	18.69	14.25	0.87	2.72	E-D	50-150
ANT138	massive peridotite	ol+cpx/opx +sp	18.6	14.21	1.07	2.61	E-D	100-250

Summarized results from quantitative texture analysis at D19 beamline (ILL- Grenoble): Rw and Rb are reliability factors related to texture analysis; F2 factor is strength factor of the recalculated texture; GoF = Goodness of Fit. LPO type refers to texture types described in the text.

Figure 7. Experimental vs. Recalculated pole figures of olivine selected crystallographic planes orientations (mrd = multiple of random distribution).

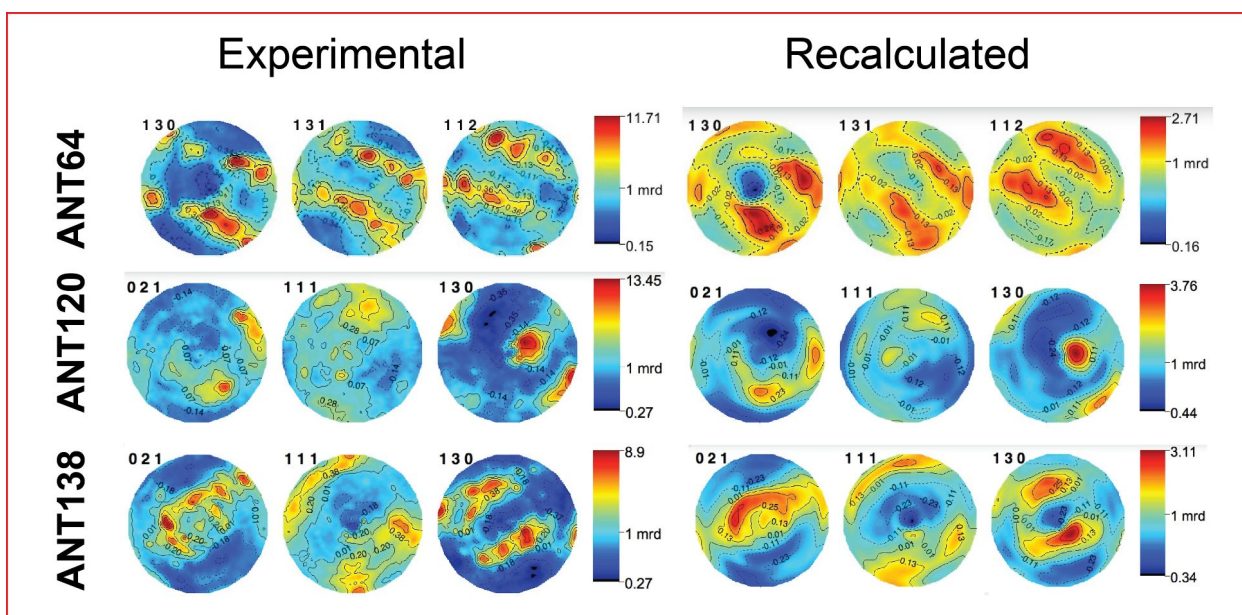
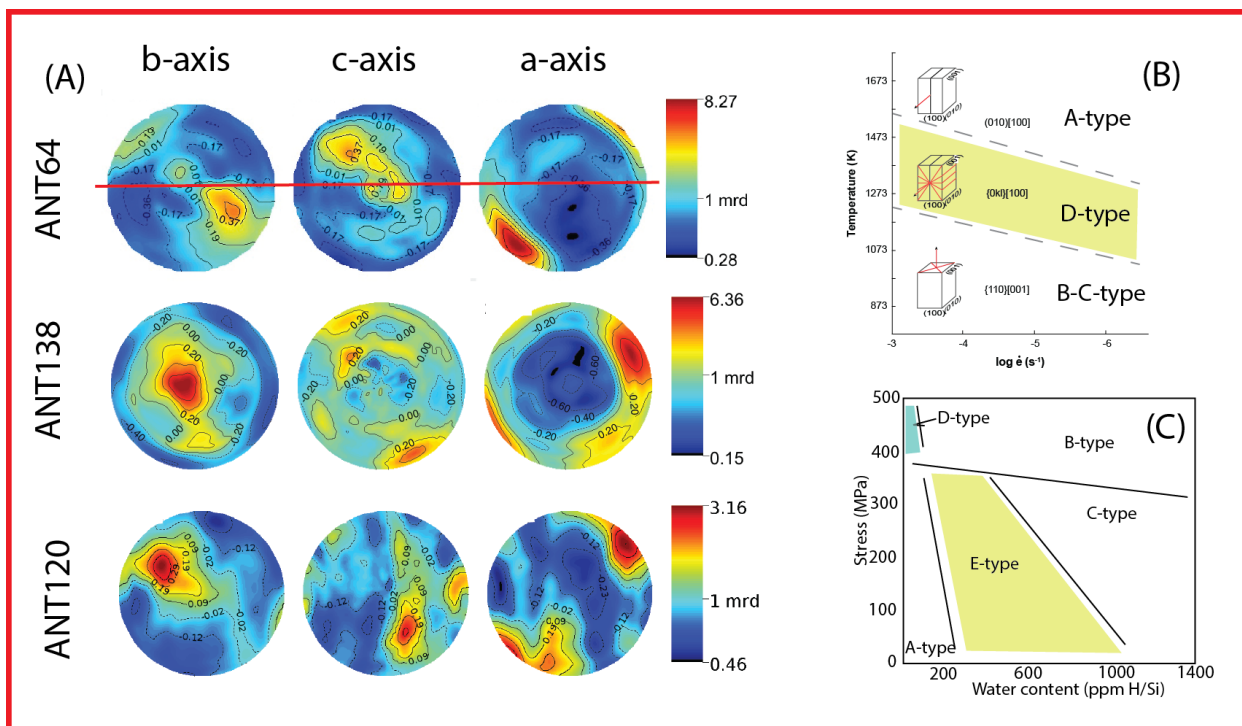


Figure 8. Main olivine texture types and their relations with stress, strain, temperature and water content.



A) Recalculated pole figure of main crystallographic planes of olivine (mrd = multiple of random distribution). B) Strain rate vs. temperature diagram showing the dominant slip systems in olivine (from Carter & Ave' Lallemand, 1970). C) Water content vs. stress diagram for olivine after Karato (2008 and references therein).

In figure 7 PFs for selected lattice planes of olivine are shown in equal-area projection. For clarity, not all the pole figures are shown though all available ones were used to refine the ODF (Orientation Distribution Function; see Wenk, 1991). One can visually assess the goodness of the ODF solution (Toby, 2006) by the EWIMV approach, by comparison of the experimental pole figures, as extracted from experimental data, and the recalculated ones, obtained from the ODF using MAUD (Lutterotti *et al.*, 1999). Otherwise, the low R and GoF factors (Table 1) for the Rietveld global fit of the Combined Analysis are quantitatively confirming the validity of the solution. In order to discuss the results in a simpler way, we used in the following the ODF to recalculate pole figures for the principal lattice planes for olivine, (h00) - (0k0) - (00l).

ANT64

The orientation of the main crystallographic axes (Fig. 8) of olivine in ANT64 is characterized by strong maximum of the [100] axis, lying within the XZ plane and at about 40-45° to the foliation plane. The [010] and [001] pole figures exhibit distributions of the b and c-axes,

respectively, in a plane perpendicular to (XZ). These distributions reveal a main component with b and c axes roughly around 45° from Y, and two minor components. One of the latter corresponds to c-axes aligned with Y, a and b being on the equator, simply rotated by 45° around Y. Similar LPO distributions are described for natural and experimentally deformed olivine in simple-shear regime.

ANT138

In ANT138 olivine main axes exhibit a unique b alignment along Y with, however, a larger distribution than in ANT64 (Fig. 8). This larger distribution explains why both the maximum density of pole figures and F indexes are lower than in ANT64. The main component for the LPO of olivine is with a-axes at a similar orientation as ANT64 with, however, around 10-20° more towards the foliation plane. A second minor component corresponds to a-axes at 90° from the main component in the XZ plane.

ANT120

Olivine in ANT120 also displays a main LPO component with a-axes located in the XZ plane, but this latter

splits into a second and third components some ten degrees off XZ. B-axes are like in ANT138 distributed around a single pole, but not centered on Y. The overall texture strength is lower than in the two other samples, due to both the dispersion of the components and splits. Such mixed distribution may be related to intracrystalline deformation occurring in large olivine grains as shown at the microscopic scale. It is likely that the original distribution is partly dispersed as consequence of intracrystalline creep as testified by undulose extinction and subgrains. As discussed previously, sample ANT120 is not characterised by meso- and microscopic planar or linear structures.

Discussion

Serpentinized peridotites with minor interbedded mafic-ultramafic rocks, namely, cm-scale cpx-rich layers, amp-bearing chloriteschists, dunite, amphibole-rich layers, and chloriteschists constitute the sole for the volcanic and cover sequence of the Antrona ophiolites (see also Tartarotti *et al.*, 2011). A multi-scalar structural study here performed on selected samples of the Antrona ultramafic rocks reveals the occurrence of relict microstructures, textures and mineralogy attributable to a pre-Alpine oceanic origin, prior to the dominant Alpine tectonometamorphic imprint affecting the whole ophiolite sequence and well-documented in the literature (Colombi and Pfeifer, 1986; Colombi, 1989; Pfeifer *et al.*, 1989; Turco and Tartarotti, 2006).

The ultramafic portion of the Antrona ophiolite mostly consists of foliated serpentinites which preserve pre-Alpine mantle porphyroclastic textures (see Figs. 3), although crystal-plastic recrystallization with neoblasts formation related to the Alpine orogenic history has likely occurred. Olivine represents the best preserved mineral phase and is here interpreted as mantle relic, as suggested by its microstructural and textural features. Intracrystalline deformation may also be inferred by the occurrence of subgrains (see Figs. 3c, 3d) and deformation lamellae inside olivine porphyroblasts, commonly found in mantle tectonic peridotites (Den Tex, 1969; Mercier and Nicolas, 1975). These and other microstructures typical of mantle peridotites, such as exsolved clinopyroxene porphyroclasts, and porphyroclastic holly-leaf-shaped spinel (e.g. Gueguen and Nicolas, 1980; Tartarotti *et al.*, 2002;

Dick *et al.*, 2010) were observed not only in serpentinized peridotites but also in dunite samples and in coarse-grained ol-cpx-spl-rich rocks (see Fig. 3). Dunite layers in the Antrona serpentinites can thus be interpreted as being residual rocks hosted in the mantle harzburgite/lherzolite main body. Tartarotti *et al.* (2011) have shown that olivine and clinopyroxene compositions in the Antrona serpentinites are comparable with those of abyssal peridotites from modern oceanic lithosphere (e.g., Dick 1989; Tartarotti *et al.* 2002; Seyler *et al.*, 2003; Dick *et al.* 2010; Warren and Shimizu, 2010), inferring that the slightly higher Fe content in olivine and Ca content in clinopyroxene could be related to rock recrystallization during the Alpine orogenic evolution.

Finally, further possible evidence of relict mantle textures are: rectangular pseudomorphic aggregates of serpentine (after probable pyroxene), and the ol+chl+amp pseudomorphs replacing earlier (ortho?) pyroxene in coarse-grained ol-cpx-spl-rich rocks (see also Tartarotti *et al.*, 2011). As far as spinel crystals found in the studied ultramafic rocks, it is noteworthy the occurrence of a well preserved holly-leaf habit (recalling the typical texture of mantle peridotites), in spite of the internal reworked texture revealing a Ferritchromite composition. Similar Ferritchromite-rich spinel crystals characterized by a porous texture and a Cr-chlorite rim (like that found in our samples; see Figs. 3, 4, 5) has been described in a few localities, such as the Kalkan ophiolite of the southern Urals, and interpreted as being due to hydration and oxidation reactions consuming Al-rich chromite during prograde metamorphism (Merlini *et al.*, 2009). Other Authors (e.g. Mellini *et al.*, 2005) suggest that Ferritchromite is of hydrothermal origin formed after the oceanic serpentinization of Al-rich spinel. Ferritchromite porphyroclasts rimmed by Cr-chlorite have been recently found in the blueschist facies ophiolites of the Southern Apennine ophiolites (Sansone *et al.*, in press) and interpreted as being related to oceanic alteration. Although an oceanic origin for the studied Ferritchromite samples cannot be ruled out, further investigations, such as TEM analyses are needed in order to precisely characterize the internal structure of Ferritchromite.

In order to better constrain the origin of relict olivine in the studied samples, a Quantitative Texture Analysis (QTA) using neutron diffraction was carried out in rock samples containing olivine crystals. QTA analysis reports a well defined LPO of olivine in the three samples

though ANT64 displays the highest F2 value (3.43). Such a difference in calculated texture strength may be also referred to differences in grain-sizes (Table 1) that may influence the F2 values. Similarly the higher values of R_w , R_b and GoF observed for ANT64 do not necessarily correspond to a lower quality refinement, since the comparison of experimental and computed patterns and PFs points to a well reproduced LPO. The discrepancies may be due to several factors as grain-size variations and presence of other mineral phases in the analysed rocks as well the shape of the analysed sample with respect to the D19 setup. All these factors may imply an increase of the refinement factors (Chateigner, 2005; Toby, 2006).

The relationship between the olivine LPO and the dominant slip system may be inferred if meso- or microscopic shear planes are visible and may be used as reference to compare natural LPO with experimental or theoretical LPO (Jung and Karato, 2001; Karato, 2008). Olivine LPO in sample ANT64 displays orientations similar to those described by several authors as characteristic of type D and E distribution (Drury, 2005; Karato *et al.*, 2008 and reference therein; Tartarotti *et al.*, 2011; Tommasi *et al.*, 2000). Similar patterns, comparable with type E distribution, are also present in samples ANT138 and ANT120 olivine, albeit the absence of a clearly defined mesoscopic foliation reduces the reliability of the comparison.

This comparison suggests slip systems $[100](0kl)$ and $[100](001)$ as active slip systems in the studied samples (Karato *et al.*, 2008), which require $T > 800^\circ\text{C}$ for $P = 1.5$ for the activation (Carter and Ave'lallemant, 1970) and a relatively low content (< 800 ppm H/Si) of water in olivine (Jung and Karato, 2001; Karato, 2008).

Since the relationship between olivine fabric and the dominant slip systems suggests $[100](0kl)$ and $[100](001)$ as active slip systems (Karato *et al.*, 2008) and the activation of these slip systems is referred as possible at $T > 800^\circ\text{C}$ for $P = 1.5$ GPa (Carter and Ave'lallemant, 1970), although it is sensitive to a pressure increase (e.g., Raterron *et al.*, 2009), we confirm a mantle origin for the olivine fabric, as inferred by Tartarotti *et al.* (2011), inherited from the pristine mantle structure. An origin of the olivine LPO related to the Alpine evolution is discarded since temperature values as high as 800°C have never been estimated for the Antrona ophiolites.

Moreover, the development of D-type olivine LPO is considered to be a sign of the presence of a moderate

amount of water in mantle olivine crystals ($< 800\text{H/Si}$ ppm after Paterson, 1982). Such an amount of water is considered to be relevant for style in tectonics, having implications for the mechanics of subduction processes, by switching on highly localized weak faulting instead of a broad, slow creeping flow (Regenauer-Lieb, 2003), the transition occurring above a water concentration of 200 ppm H/Si.

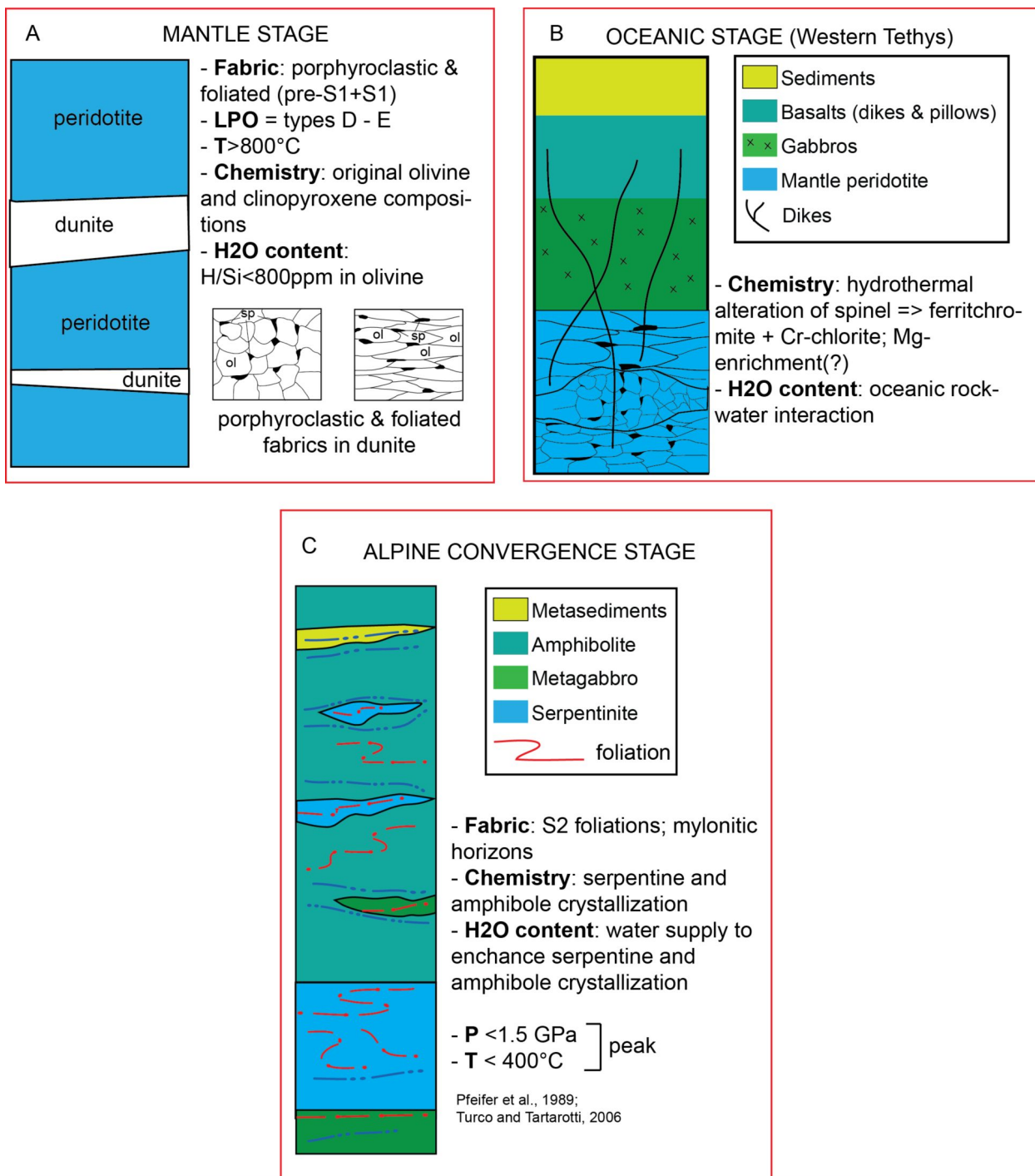
This interaction and incorporation of water within olivine crystal defects may have occurred before oceanic alteration, where further water is interacting with olivine and other rock-forming minerals as suggested by chemical reactions and X-rays chemical maps in spinel domains (see Figs. 4, 5).

Other serpentinite bodies in the Alpine metaophiolites, namely, the Mount Avic serpentinites (Tartarotti and Martin, 1991; Diella *et al.*, 1994; Fontana *et al.*, 2008), the Zermatt-Saas serpentinites (Li *et al.*, 2004), and the southern Lanzo ophiolitic massif (e.g., Piccardo *et al.*, 2005) have been interpreted as being of oceanic origin, although not supported by quantitative fabric analyses. During the Alpine evolution, mylonitised serpentinites developed due to strain gradients and most of the earlier fabrics have been erased, leading to structural transposition of early S_1 foliation consisting of porphyroblastic olivine, clinopyroxene, spinel, and serpentine and formation of S_2 foliation. Conversely, within low strain volumes, serpentinites and host dunite and other ultramafic rocks could partly preserve their original structure.

Summary and conclusions

The Antrona ultramafic body derives from mantle harzburgites - lherzolites associated with dunite pods (\pm pyroxenite layers; Fig. 9a). The LPO of olivine and the chemical composition of olivine, clinopyroxene porphyroblasts and spinel suggests a sub-oceanic nature for these mantle-derived rocks. Though the Alpine tectonic transposition has obliterated the primary structure of the Tethyan lithosphere, thus preventing a clear interpretation of the original stratigraphy, however we envisage that the mantle portion of the Antrona ophiolite may have constituted a section of the Jurassic Tethyan oceanic lithosphere, together with gabbros, basalts and sediments (Fig. 9b), now constituting the highly strained amphibolite, metagabbro and metasedimentary horizons (Fig. 9c).

Figure 9. Simplified model of the evolution of the Antrona Ophiolite, from mantle to Alpine convergence stage.



Except for the scarce occurrence of rodingites in the Antrona area, this scenario is comparable to that envisaged for the Mount Avic serpentinite massif (Tartarotti and Martin, 1991; Fontana *et al.*, 2008; Panseri *et al.*, 2008) and although their extension is smaller, the Antrona ophiolite seems to be comparable with a coherent ophiolitic slice, such as the Zermatt Saas ophiolite (e.g., Angiboust *et al.*, 2011 and refs. therein), more than with

a serpentinite mélangé. Turco and Tartarotti (2006) suggest for amphibolites a P-T evolution characterized by early Alpine prograde blueschist path (T = 372° C for P = 1 GPa), followed by an eclogitic metamorphic stage (T = 386° C for P = 1.5 GPa), which was further followed by a decompression accompanying the exhumation history in the Tertiary (Pfeifer *et al.* 1989; Turco and Tartarotti, 2006), testified by a re-equilibration under epidote

amphibolite to amphibolite facies conditions. A similar P-T evolution may be indicatively addressed for clinopyroxene-rich layers and amp-bearing chloriteschists, probably originated by original gabbros transformed during the Alpine tectonics.

Acknowledgements

Sax Mason (ILL Grenoble) is warmly thanked for the kind assistance at D19. Daniel Chateigner is thanked for his careful review.

References

- Angiboust S., Agard P., Jolivet L. and Beyssac O., 2009. The Zermatt-Saas ophiolite: the largest (60-km wide) and deepest (c. 70-80 km) continuous slice of oceanic lithosphere detached from a subduction zone? *Terra Nova*, 21: 171-180.
- Argand E., 1911. Le nappes de recouvrement des Alpes occidentales et les territoires environnants. Essai de carte structurale 1:500.000. Carte spéc. N.64 avec 3 planches de profils.
- Barnicoat A.C. and Fry N., 1986. High-pressure metamorphism of the Zermatt-Saas ophiolite zone, Switzerland. *Journal of the Geological Society*, 143: 607-618.
- Bearth P., 1954. Geologischer Atlas der Schweiz 1:25.000, Blatt Saas (Nr. 30) und Blatt Monte Moro (Nr. 31). Schweiz. Geol. Kommission.
- Bearth P., 1956. Zur geologie der Wurzelzone östlich des Ossolatales. *Eclogae Geologicae Helveticae*, 49: 267-278.
- Bigioggero B., Boriani A., Colombo A. and Tunesi A., 1981. Età e caratteri petrochimici degli ortogneiss della zona Moncucco-Orselina nell'area Ossolana. *Rendiconti della Società Italiana di Mineralogia e Petrologia*, 38: 207-218.
- Bucher K., Fazis Y., de Capitani C., and Grapes R., 2005. Blueschists, eclogites, and decompression assemblages of the Zermatt-Saas ophiolite: High-pressure metamorphism of subducted Tethys lithosphere. *American Mineralogist*, 90: 821-835.
- Bunge H.J. and Esling C., 1982. Quantitative Texture Analysis (551 pp.). Deutsche Gesellschaft für Metallkunde. 551pp.
- Bunge H.J., Wenk H.R. and Pannetier J., 1982. Neutron diffraction texture analysis using a 2 θ position sensitive detector. *Textures and Microstructures*, 5: 153-170.
- Camana G., Chateigner D., Zucali M., Artioli G., 2002. The grid-work texture of authigenic microcrystalline quartz in siliceous crust-type (SCT) mineralized horizons. *American Mineralogist*, 87, 1128-1138
- Carrupt E. and Schlup M., 1998. Métamorphisme et tectonique du versant sud du Val Bognanco (Pennique, Alpes italiennes). *Bulletin de la Société Vaudoise des Sciences Naturelles*, 86: 29-59.
- Carter N.L. and Ave'llemant H.G., 1970. High temperature flow of dunite and peridotite. *Geological Society of America Bulletin*, 81: 2181-2202.
- Chateigner, D., 2005, Reliability criteria in quantitative texture analysis with experimental and simulated orientation distributions: *Journal of Applied Crystallography*, v. 38, p. 603-611.
- Chateigner D., 2010. Combined Analysis. ISTE Ltd and John Wiley & Sons Inc, 496 pp.
- Colombi A., 1989. Métamorphisme et géochimie des roches mafiques des Alpes ouest-centrales (géoprofil Viège-Domodossola-Locarno). *Mémoires de Géologie, Lausanne*, 4: 1-216.
- Colombi A. and Pfeifer H.-R., 1986. Ferrogabbroic and basaltic meta-eclogites from the Antrona mafic-ultramafic complex and the Centovalli-Locarno region (Italy and Southern Switzerland) – first results. *Schweizerische Mineralogische und Petrographische Mitteilungen*, 66: 99-110.
- Den Tex E., 1969. Origin of ultramafic rocks, their tectonic setting and history: a contribution to the discussion of the paper: "The origin of ultramafic and ultrabasic rocks" by P.J. Wyllie. *Tectonophysics*, 7: 457-488.
- Dick H.J.B., 1989. Abyssal peridotites, very slow spreading ridges and oceanic ridge magmatism. In: A.D. Sanders and M.J. Morris (Eds.), *Magmatism in the ocean basins*, Geological Society, London, Special Publications 42, p. 71-105.
- Dick H.J.B., Lissenberg C.J. and Warren J.M., 2010. Mantle melting, melt transport, and delivery beneath a slow-spreading ridge: the Paleo-MAR from 23°15'N to 23°45'N. *Journal of Petrology*, 51: 425-467.
- Diella V., Ferrario A. and Rossetti P., 1994. The magnetite ore deposits of the southern Aosta valley: chromitite transformed during an Alpine metamorphic event. *Ophioliti*, 19: 247-256.
- Drury M.R., 2005. Dynamic recrystallization and strain softening of olivine aggregates in the laboratory and the lithosphere. *Geological Society of London, Special Publication*, 243: 143-158.
- Ernst W. G. and Dal Piaz G.V., 1978. Mineral parageneses of eclogitic rocks and related mafic schists of the Piemonte ophiolite nappe, Breuil-St.Jacques area, Italian Western Alps. *American Mineralogist*, 63: 621-640.
- Escher A., Hunziker J.C., Marthaler M., Masson H., Sartori M. and Steck A., 1997. Geologic framework and structural evolution of the western Swiss-Italian Alps. In: O.A. Pfiffner, Lehner, P., Heitzmann, P., Müller, St. and Steck A. (Eds.), *Deep structure of the Swiss Alps*, Birkhäuser Verlag, Basel, p. 205-221.
- Fontana E., Panseri M. and Tartarotti P., 2008. Oceanic relict textures in the Mount Avic serpentinites, Western Alps. *Ophioliti*, 33: 105-118.
- Froitzheim N., 1997. Mesozoic paleogeography and Alpine tectonics along transects in eastern and western Switzerland – Consequences of the origin of the Monte Rosa nappe. 3rd Workshop on Alpine Geological Studies. *Quaderni di Geodinamica Alpina e Quaternaria*, 4: 53-54.
- Froitzheim N., 2001. Origin of the Monte Rosa nappe in the Pennine Alps – A new working hypothesis. *Geological Society of American Bulletin*, 113: 604-614.

- Gatta, G. D., N. Rotiroti, and M. Zucali, 2009. Plastic deformations in kyanites by tectonometamorphic processes: a single-crystal X-ray diffraction study. *Mineralogical Magazine*: 73, 359.
- Gueguen Y. and Nicolas A., 1980. Deformation of mantle rocks. *Annual Review of Earth and Planetary Sciences*, 8: 119-144.
- Heitzmann J.J. and Laruelle C. (1986). Simultaneous measurement of several X-ray pole figures. *Journal of Applied Crystallography*, 19: 467-472.
- Jaboyedoff M., Bégli P. and Lobrinus S., 1996. Stratigraphie et évolution structurale de la zone de Furgg, au front de la nappe du Mont-Rose. *Bulletin de la Société Vaudoise des Sciences Naturelles*, 84: 191-210.
- Jung, H., and Karato, S., 2001, Water-induced fabric transitions in olivine: *Science*, v. 293, p. 1460-1463.
- Karato S., 2008. Deformation of Earth materials: an introduction to the rheology of solid Earth, Cambridge University Press, 463 pp.
- Karato S., Jung H., Katayama I. and Skemer P., 2008. Geodynamic significance of seismic anisotropy of the upper mantle: new insights from laboratory studies. *Annual Review of Earth and Planetary Sciences*, 36, 59 pp.
- Keller L.M. and Schmid S.M., 2001. On the kinematics of shearing near the top of the Monte Rosa nappe and the nature of the Furgg zone in Val Loranco (Antrona valley, N. Italy). *Tectonometamorphic and paleogeographical consequences*. *Schweizerische Mineralogische und Petrographische Mitteilungen*, 81: 347-367.
- Keller L.M., Hess M., Fügenschuh B. and Schmid S.M., 2005a. Structural and metamorphic evolution of the Camughera-Moncucco, Antrona and Monte Rosa units southwest of the Simplon line, Western Alps. *Eclogae Geologicae Helvetiae*, 98: 21-52.
- Keller L.M., Abart R., Schmid S.M. and De Capitani C., 2005b. Phase Relations and Chemical Composition of Phengite and Paragonite in Pelitic Schists During Decompression: a Case Study from the Monte Rosa Nappe and Camughera-Moncucco Unit, Western Alps. *Journal of Petrology*, 46: 2145-2166.
- Kramer J., 2002. Structural evolution of the Penninic Units in the Monte Rosa region (Swiss and Italian Alps). Ph.D. Dissertation, University of Basel, Switzerland, 154 pp.
- Laduron D., 1976. L'antiforme de Vanzone. Etude pétrologique et structurale dans la Valle Anzasca (Province de Novara, Italie). *Mémoire de l'Institut de Géologie, Université Louvain*, 121 pp.
- Laduron D. and Merlin M., 1974. Evolution structurale et métamorphique de l'antiforme de Vanzone (Valle Anzasca, Prov. de Novara, Italie). *Bulletin de la Société Géologique de France*, 16: 264-265.
- Li X.P., Rahn M. and Bucher K., 2004. Serpentinites of the Zermatt-Saas ophiolite complex and their texture evolution. *Journal of Metamorphic Geology*, 22: 159-177.
- Lutterotti, L., Matthies, S., and Wenk, H. R., 1999. MAUD (Material Analysis Using Diffraction): a user friendly Java program for Rietveld Texture Analysis and more: *Proceedings of the Twelfth International Conference on Textures of Materials (ICOTOM-12)*, v. 2, p. 1599.
- Liu, Y., Wang, F., Xu, J., and Liang, Z., 1993, Estimation of the true orientation distribution function determination of the maximum-entropy method by the Taylor model: *Journal of Applied Crystallography*, v. 26, p. 268-271.
- Martin S., Tartarotti P. and Dal Piaz G.V., 1994. The Mesozoic ophiolites of the Alps: A review. *Boll. Geofisica Teorica e Applicata*, 36: 175-219.
- Matthies S., Lutterotti L. and Wenk H.R., 1997. Advances in Texture Analysis from Diffraction Spectra. *Journal of Applied Crystallography*, 30: 31-42.
- Mellini M., Rumori C. and Viti C., 2005. Hydrothermally reset magmatic spinels in retrograde serpentinites: formation of "ferritchromit" rims and chlorite aureoles. *Contributions to Mineralogy and Petrology*, 149: 266-275.
- Mercier J.-C. C. and Nicolas A., 1975. Textures and Fabrics of Upper-Mantle Peridotites as Illustrated by Xenoliths from Basalts. *Journal of Petrology*, 16: 454-487.
- Merlini A., Grieco G. and Diella V., 2009. Ferritchromite and chromian-chlorite formation in mélange-hosted Kalkan chromitite (Southern Urals, Russia). *American Mineralogist*, 94: 1459-1467.
- Milnes A.G., Grellier M. and Müller R., 1981. Sequences and style of major post-nappe structures, Simplon-Pennine Alps. *Journal of Structural Geology*, 3: 411-420.
- Morawiec A., 2004. Orientations and rotations: computations in crystallographic textures, Springer Verlag, 210 pp.
- Nicolas A. and Poirier J.P., 1976. Crystalline Plasticity and Solid State Flow in Metamorphic Rocks, John Wiley & Sons, London, 444 pp.
- Oberhänsli R., 1980. P-T Bestimmungen anhand von Mineralanalysen in Eklogiten und Glaukophaniten der Ophiolite von Zermatt. *Schweizerische Mineralogische und Petrographische Mitteilungen*, 60: 215-235.
- Panseri M., Fontana E. and Tartarotti P., 2008. Evolution of rodingitic dykes: metasomatism and metamorphism in the Mount Avic serpentinites (Alpine Ophiolites, southern Aosta Valley). *Ophioliti*, 33: 165-185.
- Paterson, M. S., 1982, The determination of hydroxyl by infrared absorption in quartz, silicate glass and similar materials. *Bull. Mineral.*, 105: 20-29.

- Pfeifer H.R., Colombi A. and Ganguin J., 1989. Zermatt-Saas and Antrona zone: A petrographic and geochemical comparison of polyphase metamorphic ophiolites of the western-central Alps. *Schweizerische Mineralogische und Petrographische Mitteilungen*, 69: 217-236.
- Piccardo G.B., Zanetti A., Spagnolo G. and Poggi E., 2005. Recent researches on melt-rock interaction in the Lanzo South peridotite. *Ophioliti*, 30: 135-160.
- Regenauer-Lieb, K., Yuen, D. A., and Branlund, J., 2001, The initiation of subduction: Criticality by addition of water? *Science*, 294: 578-580.
- Raterron P., Amiguet E., Chen J., Li L. and Cordier P., 2009. Experimental deformation of olivine single crystals at mantle pressures and temperatures. *Physics of the Earth and Planetary Interiors*, 172: 74-83.
- Reinecke T., 1991. Very-high-pressure metamorphism and uplift of coesite-bearing metasediments from the Zermatt-Saas zone, Western Alps. *European Journal of Mineralogy*, 3: 7-17.
- Reinecke T., 1998. Prograde high to ultrahigh pressure metamorphism and exhumation of oceanic sediments at Lago di Cignana, Zermatt Saas Zone, western Alps. *Lithos*, 42: 147-190.
- Sansone M.T.C., Prosser G., Izzo G., and Tartarotti P., 2012. Spinel-peridotites of the Frido Unit ophiolites (Southern Apennine-Italy): evidence for oceanic evolution. *Periodico di Mineralogia*, 81, in press.
- Seyler M., Cannat M. and Mével C., 2003. Evidence for major-element heterogeneity in the mantle source of abyssal peridotites from the Southwest Indian Ridge (52° to 68°E). *Geochemistry, Geophysics, Geosystems*, 4(2), 10.1029/2002GC000305
- Steck A., Epard J.-L., Escher A., Lehner P., Marchant R. and Masson H., 1997. Geological interpretation of the seismic profile through Western Switzerland: Rawil (W1), Val d'Anniviers (W2), Matteredal (W3), Zmutt-Zermatt-Findelen (W4) and Val de Bagnes (W5). In O.A. Pfiffner, P. Lehner, P. Heitzmann, St. Müller, & A. Steck (Eds.), *Deep structure of the Swiss Alps*, Birkäuser Verlag, Basel, pp. 123-137.
- Steck A., Epard J.-L., Escher A., Gouffon Y. and Masson H., 2001. Carte tectonique des Alpes de Suisse occidentale et des régions avoisinantes 1:100,000. Notice explicative, Office fédérale des eaux et de la géologie, 73 pp.
- Tartarotti P. and Martin S., 1991. Ultramafic rocks in the Mount Avic eclogitic ophiolites, Italian Western Alps. *Terra Abstracts*, 3, p. 96.
- Tartarotti P., Susini S., Nimis P. and Ottolini L., 2002. Melt migration in the upper mantle along the Romanche Fracture Zone (Equatorial Atlantic). *Lithos*, 63: 125-149.
- Tartarotti P., Zucali M., Panseri M., Lissandrelli S., Capelli S., and Bachir O., 2011. Mantle origin of the Antrona serpentinites (Antrona ophiolites, Pennine Alps) as inferred from microstructural, microchemical, and neutron diffraction quantitative texture analysis. *Ophioliti*, 36(2): 167-189.
- Tommasi A., Mainprice D., Canova G. and Chastel Y., 2000. Viscoplastic self-consistent and equilibrium-based modeling of olivine lattice preferred orientations: Implications for the upper mantle seismic anisotropy. *Journal of Geophysical Research-Solid Earth*, 105: 7893-7908.
- Turco F. and Tartarotti P., 2006. The Antrona nappe: lithostratigraphy and metamorphic evolution of ophiolites in the Antrona Valley (Pennine Alps). *Ophioliti, Special Issue "Modern and fossil oceanic lithosphere"*, 31: 207-221.
- Toby, B. H., 2006, R factors in Rietveld analysis: How good is good enough?: *Powder diffraction*, v. 21, p. 67-70. 10.1154/1.2179804
- Ullemeyer K., Spalhoff P., Heinitz J., Isakov N.N., Nikitin A.N. and Weber K., 1998. The SKAT texture diffractometer at the pulsed reactor IBR-2 at Dubna: experimental layout and first measurements. *Nuclear Instruments Methods in Physics Research A*, 412: 80-88.
- Warren J.M. and Shimizu N., 2010. Cryptic variations in abyssal peridotite compositions: evidence for shallow-level melt infiltration in the oceanic lithosphere. *J. Petrology*, 51: 395-423.
- Warren J.M., Hirth G., Kelemen P.B. 2008. Evolution of olivine lattice preferred orientation during simple shear in the mantle. *Earth and Planetary Science Letters* 272 (2008) 501-512.
- Wenk H.R., 1985. Preferred orientation in deformed metals and rocks; an introduction to modern texture analysis, Orlando, FL, United States, Acad. Press, 610 pp.
- Wenk H-R., 1991. Standard project for pole figure determination by neutron diffraction. *Journal of Applied Crystallography*, 24: 920-927.
- Wenk H.R., Matthies S., Lutterotti L., 1994. Texture analysis from diffraction spectra. *Materials Science Forum*, 157: 473-480.
- Zucali, M., Chateigner, D., Dugnani, M., Lutterotti, L., and Ouladdiaf, B., 2002, Quantitative texture analysis of naturally deformed hornblendite under eclogite facies conditions (Sesia-Lanzo Zone, Western Alps): comparison between x-ray and neutron diffraction analysis. In: De Meer, S., Drury, M.R., De Bresser, J.H.P., and Pennock, G.M., ed., *Deformation Mechanisms, Rheology and Tectonics: Current Status and Future perspectives*. Geological Society of London Special Publications. 200: p. 239-253.

Zucali, M., V. Barberini, D. Chateigner, B. Ouladdiaf, and L. Lutterotti, 2010: Brittle plus plastic deformation of gypsum aggregates experimentally deformed in torsion to high strains: quantitative microstructural and texture analysis from optical and diffraction data. From: SPALLA, M. I., MAROTTA, A. M. & GOSSO, G. (eds) *Advances in Interpretation of Geological Processes: Refinement of Multi-scale Data and Integration in Numerical Modelling*. Geological Society, London, Special Publications, 332, 79–98. 10.1144/SP1332.1146 0305-8719/1110